The impacts of optimizing model-dependent parameters on the Antarctic sea ice data assimilation

Hao Luo[1], Qinghua Yang[1], Matthew Mazloff[2], Lars Nerger[3], and Dake Chen[1,4]

[1]School of Atmospheric Sciences, Sun Yat-sen University, and Southern Marine Science and Engineering Guangdong Laboratory (Zhuhai), Zhuhai 519082, China.

[2]Scripps Institution of Oceanography, University of California, San Diego, CA, USA

[3]Alfred Wegener Institute, Helmholtz Centre for Polar and Marine Research, Bremerhaven 27570, Germany

[4]State Key Laboratory of Satellite Ocean Environment Dynamics, Second Institute of Oceanography, Ministry of Natural Resources, Hangzhou 310012, China

Corresponding author: Qinghua Yang (yangqh25@mail.sysu.edu.cn)

Key points:

- Refining localization and observation error estimate raises the Antarctic sea ice modeling obtained by assimilating sea ice concentration
- Assimilating sea ice concentration can constrain the modeling of Antarctic sea ice volume except for its modeling uncertainty
- More oceanic and sea-ice observations are required for the reconstruction of Antarctic sea ice

Abstract

Given the role played by the historical and extensive coverage of sea ice concentration (SIC) observations in reconstructing the long-term variability of Antarctic sea ice, and the limited attention given to model-dependent parameters in current sea ice data assimilation studies, this study focuses on enhancing the performance of the Data Assimilation System for the Southern Ocean (DASSO) in assimilating SIC through optimizing the localization and observation error estimate, and two assimilation experiments were conducted from 1979 to 2018. By comparing the results with the sea ice extent of the Southern Ocean and the sea ice thickness in the Weddell Sea, it becomes evident that the experiment with optimizations outperforms that without optimizations due to achieving more reasonable error estimates. Investigating uncertainties of the SIV anomaly modeling reveals the nonnegligible role played by the sea ice-ocean interaction during the SIC assimilation, implying the necessity of assimilating more oceanic and sea-ice observations.

Plain Language Summary

Antarctic sea ice is essential for the Earth's system, but its variability is challenging to understand due to limited observations and model limitations. Data assimilation, a method combining observations and simulations, can help address these challenges. To better incorporate long historical sea ice concentration (SIC) observations, we improved the Data Assimilation System for the Southern Ocean (DASSO) by refining the model-dependent parameters of assimilation in this study. We conducted experiments from 1979 to 2018 and compared two experiments with and without optimizations. The results demonstrate the reliability and superiority of the experiment with optimizations compared to that without optimizations in comparison with sea ice extent in the Southern Ocean and sea ice thickness derived from the upward-looking sonar in the Weddell Sea. Further analysis shows that the relationship between sea ice and the ocean plays a nonnegligible role in assimilating SIC, which reflects the need to assimilate more oceanic and sea-ice observations to improve the Antarctic sea ice simulation. Our studies can contribute to the more reasonable reconstruction of the long-term variability of Antarctic sea ice, which benefits a better understanding of Antarctic sea ice variabilities.

1 Introduction

The understanding of Antarctic sea ice variability holds significant scientific and socioeconomic importance, owing to the crucial role that Antarctic sea ice plays in the Earth system (Turner & Comiso, 2017). Nonetheless, the present sparsity of sea ice observations poses a challenge in achieving a comprehensive understanding of the Antarctic sea ice system (e.g., J. Wang, Min, et al., 2022; Worby et al., 2008), and numerical models currently exhibit notable limitations in adequately capturing the variations in Antarctic sea ice (e.g., Shu et al., 2020; Tsujino et al., 2020). Consequently, data assimilation has emerged as a valuable approach, as it synergistically combines information from both observations and simulations. This integrative approach facilitates a more profound investigation into the complexities of Antarctic sea ice variability and represents a critical step towards enhancing the accuracy of Antarctic sea ice prediction.

Given the limited availability of Antarctic sea ice observations and the challenges associated with data acquisition, substantial efforts have been dedicated to constraining the Antarctic sea ice system through assimilating long historical sea ice concentration (SIC) data using assimilation algorithms of varying complexities (e.g., Massonnet et al., 2013; Mazloff et al., 2010; J. Zhang & Rothrock, 2003). Previous studies have demonstrated the enhancement of Antarctic sea ice simulation achieved through SIC assimilation, leading to the widespread use of corresponding sea ice reanalyses. However, recent evaluations, which take into account the emergence of additional Antarctic sea ice observations, reveal that significant uncertainties persist to some extent in these reanalyses (e.g., Nie et al., 2022; Shi et al., 2021). While assimilating more sea ice observations has the potential to further improve the simulation of Antarctic sea ice (e.g., Luo et al., 2021; Massonnet et al., 2014), the historical and extensive coverage of SIC observations makes them indispensable for reconstructing the long-term variability of Antarctic sea ice.

In theory, the truth of data assimilation is defined in the space of the model (Lewis et al., 2006), which consequently renders several parameters of data assimilation reliant on the model's intrinsic characteristics during practical application. However, current studies on sea ice data assimilation, including our previous study (Luo et al., 2021), frequently overlook these model-dependent parameters to a certain degree. For instance, the implementation of localization in ensemble-based data assimilation aims to diminish spurious correlations across extensive spatial distances, and the localization radius should be varied with background error covariance matrices produced by different models. Regrettably, current practices in sea ice data assimilation commonly rely on fixed localization radius derived from empirical insights. In addition, observation errors utilized in data assimilation consist of both measurement errors and representation errors. Representation errors arise from physical processes and scales that are observable through measurements but not adequately resolved by numerical models (Oke & Sakov, 2008). For instance, fine structures of sea ice, such as sea ice leads and edges, significantly impact the state of sea ice (Maykut, 1978). However, the coarse resolution of current sea ice models impedes their ability to effectively capture these intricate features, thereby introducing representation errors. Unfortunately, in current sea ice data assimilation, observation errors tend to focus primarily on accounting for measurement errors while ignoring the contribution of representation errors to some degree.

Therefore, the question remains as to whether calibrating model-dependent parameters in data assimilation can enhance the performance of sea ice data assimilation. In this study, we further refine the existing Data Assimilation System for the Southern Ocean (DASSO) and investigate the impact of these optimizations on the assimilation of SIC observations.

2 Methodology

2.1 Description on DASSO

DASSO has been developed by utilizing the Massachusetts Institute of Technology general circulation model (MITgcm, Marshall et al., 1997) and the Parallel Data Assimilation Framework (PDAF, Nerger & Hiller, 2013). The model configuration is identical to that used by Verdy and Mazloff (2017). At present, DASSO successfully assimilates SIC and sea ice thickness (SIT) observations (Luo et al., 2021), employing the Local Error Subspace Transform Kalman Filter (LESTKF, Nerger et al., 2012). Another recent breakthrough in DASSO pertains to the development of a multivariate balanced atmospheric ensemble forcing (Luo et al., 2023), which not only enhances the accuracy of simulations but also leads to a more reasonable estimation of simulation uncertainties, serving as the cornerstone for further optimization of DASSO.

2.2 Optimization of DASSO

To optimize the localization radius and the estimate of observation error variance employed in DASSO, an ensemble simulation from 1979 to 2018 is conducted without data assimilation. This ensemble simulation is forced by the abovementioned multivariate balanced atmospheric ensemble forcing, and its initial condition is perturbed using second-order exact sampling (Pham, 2001) based on daily output from a free run of 3 months before 1 January 1979.

In this study, the localization radius is determined as the correlation length scale that best fits the Gaspari and Cohn function (Gaspari & Cohn, 1999), and the correlation length scale is estimated based on the ensemble mean of SIC which is sampled every 5 longitudes and 1 latitude intervals in the region south of 48°S. Figure 1a illustrates the latitude-dependent variation of the localization radius for DASSO. The localization radius decreases consistently with latitude, which aligns with the variation of the Rossby deformation radius. Notably, the localization radius drops rapidly from 1633.1 km at 48°S to 698.7 km at 59°S, while it changes relatively slow south of 59°S, with the localization radius maintaining around 668.5 km. Additionally, zonal uncertainties in the localization radius are smaller south of 59°S and larger north of 59°S, suggesting that the difference in localization radius among sectors of the Southern Ocean also varies with latitude. More importantly, the mean change in the localization radius with latitude (64.9 km/degree) is larger than that with longitude (39.7 km/degree), indicating a weaker relationship between the localization radius and longitude. In light of these findings, the variation of the localization radius with latitude is considered in the DASSO through a Gaussian function.

Given the role that representation errors of observation play in sea ice data assimilation, an ensemble-based method originally proposed by Rodwell et al. (2016) for the reliability budget is employed to estimate the variances of observation error in SIC, which takes into account both the measurement error and representation error and is determined by the following equation:

$$observation\ error\ variance = \frac{1}{N-1}\sum_{i=1}^{N}\left(y^i - \bar{x}^i\right)^2 - \frac{1}{(N-1)N}\left[\sum_{i=1}^{N}\left(y^i - \bar{x}^i\right)\right]^2 - \frac{m+1}{(m-1)mN}\sum_{i=1}^{N}\sum_{j=1}^{m}\left(x^{ij} - \bar{x}^i\right)^2$$

where the overbar indicate the ensemble mean. In the equation, y represents the observation, while x represents the simulation. The superscripts i and j serve as indices denoting time and ensemble members, respectively. Additionally, N and M correspond to the number of time and the ensemble size, respectively. The terms on the right-hand side of the equation represent the mean-squared departure of the ensemble mean relative to the observation, bias, and ensemble variance, respectively. Figure 1b shows the spatial distribution of the variance of SIC observation error for DASSO, and this variance is a combined outcome of both the measurement error and representation error. A prominent saddle-like pattern is evident in the meridional direction, with larger variances at the edges and coastal regions of Antarctica, while relatively smaller variances prevail within the intermediate areas. Notably, differences in the distribution of observation error variance can be found among sectors of the Southern Ocean, such as the larger variance in the Weddell Sea near the north of the Antarctic Peninsula which is not found in other regions at the same latitude, indicating the necessity of adopting the observation error variance with spatial distribution. Furthermore, it is worth mentioning that the observation error variance estimated in this study is greater than that derived from the uncertainties provided by the observation data itself (Fig. S1), implying the importance of representation error for DASSO.

2.3 Experiment design

While SIT observations can be assimilated into DASSO, this study specifically focuses on assimilating SIC observations. The rationale behind this choice is based on the historical and extensive coverage of SIC observations, which meet the requirements for reconstructing the long-term variability of Antarctic sea ice. Therefore, SIC observations released by the Ocean and Sea Ice Satellite Application Facility (OSISAF), namely OSI-450 and OSI-430-b, are assimilated in two sets of experiments with 15 ensemble members in this study. The experiment period spans from 1 January 1979 to 31 December 2018. One experiment (denoted Assim) following Luo et al. (2021), adopts the fixed localization radius (i.e., 100 km) and observation error (i.e., 0.25), with the forgetting factor set at 0.5. While the other experiment (denoted Assim_opt) employed optimized localization radius and observation error variance as detailed in Sect. 2.2, alongside a forgetting factor of 0.95. It should be pointed out that as the forgetting factor decreases, the background error covariance is inflated, and the analysis heads to the observation.

In the evaluation process, the Southern Ocean SIC observation (OSI-450-a) and SIT derived from upward-looking sonar in the Weddell Sea serve as reference datasets. To ensure a robust evaluation, the results of the assimilation experiments for the first 12 months are excluded, and then the remaining results are interpolated to the corresponding observation locations for comparisons. Besides, all data are converted to monthly mean values and a 13-month moving mean is applied to monthly anomalies to focus on the low-frequency variability of Antarctic sea ice.

3 Results

Figure 2a depicts the temporal evolution of sea ice extent (SIE) climatology in the Southern Ocean. The observed SIE climatology exhibits a gradual increase from February to September, followed by a rapid decrease from September to February, revealing the asymmetric seasonal evolution of Antarctic SIE. Both experiments effectively capture this asymmetrical evolution of the SIE climatology and fall within the range of observation uncertainties. Compared with Assim_opt, the evolution of SIE climatology in Assim seems to more closely align with the observation, which can potentially be attributed to the utilization of the small observation error in Assim. The difference in SIE climatology between the simulation and the observation is presented in Fig. 2b. In both experiments, compared to the observation, the SIE climatology of the Southern Ocean is underestimated from December to March while overestimated from April to November, implying a common characteristic shared by the model utilized in this study. And it is noteworthy that differences in SIE climatology are more pronounced in Assim_opt compared to Assim, however, these disparities in Assim_opt remain within the range of observation uncertainties, thus affirming the reliability of Assim_opt. Furthermore, although significant regional variability is known to exist in the Antarctic sea ice (Liu et al., 2004), the difference in SIE climatology between the simulation and the observation in all sectors of the Southern Ocean continues to follow a similar pattern to that of the Southern Ocean as a whole. The only exception is April in the Ross Sea, where the difference between simulation and observation exceeds the range of observational uncertainties.

Figure 3a showcases the temporal evolution of the SIE anomaly in the Southern Ocean. Alongside the evident interannual fluctuations, the observed SIE anomaly also experiences an upward trend before November 2014, followed by a rapid decline until March 2017. The assimilation experiments successfully reproduce these observed variabilities, with Assim outperforming Assim_opt. The performance of the experiments, however, undergoes a reversal when considering the uncertainties associated with the simulations. The observation falls within the range of uncertainties in Assim_opt, while the uncertainties of Assim are hardly distinguishable in Fig. 3a. Further quantitative analysis of SIE anomaly simulations also supports these findings. Although the root mean squared error (RMSE) of Assim (121501 km^2) is less than that of Assim_opt (232031 km^2), the ensemble spread in Assim_opt (232,493 km2) is comparable to its RMSE, and the ensemble spread in Assim (7269 km^2) is much less than its RMSE. Similar phenomena happen across the sectors of the Southern Ocean (Tab. S1). These results suggest that the performance achieved in Assim is primarily attributed to the small forgetting factor, whereas that achieved in Assim_opt can be largely attributed to the more reasonable error estimates.

To investigate the impact of optimizations on the simulation of unobserved variables, SIT comparison is conducted between simulations and observations obtained from the upward-looking sonar (ULS) in the Weddell Sea (Fig. 3b). While the correlation coefficients are significant in both experiments, the correlation in Assim_opt is notably greater than that in Assim. Considering the RMSE, although the simulation of thin ice is better than that of thick ice in both experiments, Assim_opt outperforms Assim. When it comes to the relationship between RSME and the uncertainty of observation, the advantage of Assim_opt over Assim is further amplified. The RMSE of Assim_opt consistently remains close to the uncertainty of observation, regardless of whether it is thin ice or thick ice. Conversely, for thin ice, the RMSE of Assim is

comparable to the uncertainty of observation, while for thick ice, it significantly exceeds the uncertainty of observation.

Given the evident disparity in SIT simulation between Assim and Assim_opt, Figure 4a solely presents the temporal evolution of the sea ice volume (SIV) anomaly in the Southern Ocean provided by Assim_opt. The long-term variation of the SIV anomaly exhibits similarities to that of the SIE anomaly, which underscores the constraint of assimilating only SIC on the simulation of Antarctic sea ice. Notably, the SIV anomaly displays fewer high-frequency fluctuations compared to the SIE anomaly, indicating a longer-term memory effect of the SIV anomaly. Furthermore, the ensemble spread of SIV anomaly demonstrates noticeable changes between the 1990s and 2000s. It is larger until the late 1990s but smaller from the early 2000s onwards. Intriguingly, the ensemble spread of the SIE anomaly does not exhibit similar variations. Considering that atmospheric ensemble forcing and sea ice have already been constrained by atmospheric reanalysis and sea ice observation to some extent respectively, it becomes imperative to examine the relationship between sea ice and the ocean. Due to the important role of salinity in the high-latitude ocean, Figure 4b illustrates the correlation between SIV anomaly and the area-weighted mean Sea Surface Salinity (SSS) anomaly in the Southern Ocean (i.e., south of 55°S) for different decades. A significant positive correlation is discernible in the 1980s and 1990s, while an insignificant correlation is observed in the 2000s and 2010s, which aligns with the changes observed in the trend of SIE anomaly (Fig. S2). Moreover, based on the SIT budget provided MITgcm, a similar phenomenon can be found in the correlation between the change rates of SIV anomaly caused by the oceanic heat flux and the overall change rates of SIV anomaly. In the 1980s, the correlation stands at 0.46, while in the 1990s it slightly decreases to 0.31. In contrast, the ratio plummets significantly in the 2000s to 0.07 and further declines to -0.05 in the 2010s (Fig. 4b). These indicate the presence of decadal variability in the strength of sea ice-ocean interaction. Consequently, the larger ensemble spread of SIV anomaly in the 1980s and 1990s can, to some extent, be regarded as the joint result of the strong interaction between sea ice and the ocean and the ocean state not being properly constrained.

4 Conclusion and discussion

Recent studies have revealed the presence of significant uncertainties in certain aspects of Antarctic sea ice reanalyses obtained from the assimilation of SIC observations (e.g., Nie et al., 2022; Shi et al., 2021). However, the wealth of historical SIC observations, coupled with their extensive spatial coverage, renders them indispensable for the reconstruction of long-term Antarctic sea ice variability. Although prior studies on ocean data assimilation have already demonstrated the significance of optimizing model-dependent parameters for assimilating oceanic observations (e.g., Y. Wang et al., 2017; S. Zhang et al., 2005), limited attention has been given to this aspect in current sea ice data assimilation studies. As a result, the question of whether optimizing model-dependent parameters can enhance the effectiveness of assimilating SIC observations remains unanswered. In light of this, we have conducted further refinements to the model-dependent parameters of DASSO, including the development of a latitude-dependent localization scheme and the estimation of observation error variance of SIC which takes into account both measurement errors and representation errors. To assess the impact of these optimizations on the assimilation of SIC observations, we have conducted two sets of assimilation experiments, whose period spans from 1979 to 2018.

In the deterministic evaluation of SIE simulation, both the experiment with optimizations and that without optimizations falls within the range of observation uncertainties, indicating the reliability of the experiment with optimizations. In the probabilistic evaluation of SIE simulation, the experiment with optimizations significantly outperforms that without optimizations, which is owed to the more reasonable error estimation achieved through the optimizations. When examining the simulation of SIT derived from ULS in the Weddell Sea, the experiment with optimizations also exceeds that without optimizations in both the deterministic and probabilistic evaluations. This emphasizes the critical role of reasonable error estimation in adjusting unobserved variables during the assimilation process. Hence, our attention has been shifted towards the temporal evolution of SIV anomaly in the Southern Ocean provided by the experiment with optimizations. Intriguingly, while the evolution of SIV anomaly closely resembles that of SIE anomaly, the evolution of the ensemble spread of SIV anomaly displays noticeable deviations from that of SIE anomaly. This discrepancy may arise from the combined influence of decadal variations in sea ice-ocean interaction and the inadequately constrained state of the ocean.

Given the long memory exhibited by the SIV anomaly (Fig. 4a), it becomes paramount to explore viable approaches for reconstructing the long-term variability of Antarctic SIV reasonably. According to this study, two potential avenues are proposed to achieve this goal. Firstly, assimilating oceanic observations holds promise for advancing the reconstruction of both past and future states of Antarctic SIV, since the evident correlation between sea ice and the ocean in the 1980s and 1990s (Fig. 4b), as well as the occurrence of record-low SIE events in recent years (Liu et al., 2023; J. Wang, Luo, et al., 2022; L. Zhang et al., 2022). Secondly, the subpar performance in the simulation of thick ice (Fig. 3b) underscores the importance of assimilating additional SIT observations, especially those pertaining to thick ice such as SIT derived from ICESat/ICESat-2 and CryoSat-2 (Kacimi & Kwok, 2020; Xu et al., 2021). Furthermore, the assimilation of other types of sea ice observations, such as sea ice drift, could provide valuable insights for improving the simulation of Antarctic SIT (e.g., Massonnet et al., 2014; Mu et al., 2020). Moving forward, we will focus on refining the DASSO in these two aspects, and remain hopeful that the reanalysis generated by DASSO will contribute to solving Antarctica's sea-ice puzzle (e.g., Turner & Comiso, 2017).

Acknowledgments

This is a contribution to the Year of Polar Prediction (YOPP), a flagship activity of the Polar Prediction Project (PPP), initiated by the World Weather Research Programme (WWRP) of the World Meteorological Organization (WMO). We acknowledge the WMO WWRP for its role in coordinating this International Research activity. This study is supported by the National Natural Science Foundation of China (No. 41941009, 42006191), the National Key Research and Development Program of China (No. 2022YFE0106300), the Guangdong Basic and Applied Basic Research Foundation (No. 2020B1515020025), and the Norges Forskningsråd (grant no. 328886). We thank the National Supercomputer Center in Guangzhou for providing computing resources.

Open research

The daily OSISAF SIC data are available from http://doi.org/10.15770/EUM_SAF_OSI_0008,

http://doi.org/10.15770/EUM_SAF_OSI_NRT_2008, and http://doi.org/10.15770/EUM_SAF_OSI_0013. The Weddell Sea upward-looking sonar sea ice draft data are available at https://doi.pangaea.de/10.1594/PANGAEA.785565.

References

Gaspari, G., & Cohn, S. E. (1999). Construction of correlation functions in two and three dimensions. *Q. J. R. Meteorol. Soc.*, 125(554), 723-757. https://doi.org/doi:10.1002/qj.49712555417

Kacimi, S., & Kwok, R. (2020). The Antarctic sea ice cover from ICESat-2 and CryoSat-2: freeboard, snow depth, and ice thickness. *The Cryosphere*, 14(12), 4453-4474. https://doi.org/10.5194/tc-14-4453-2020

Lewis, J. M., Lakshmivarahan, S., & Dhall, S. (2006). *Dynamic data assimilation: A least squares approach*. (Vol. 13). Cambridge, UK: Cambridge University Press.

Liu, J., Curry, J. A., & Martinson, D. G. (2004). Interpretation of recent Antarctic sea ice variability. *Geophys. Res. Lett.*, 31(2), L02205. https://doi.org/10.1029/2003gl018732

Liu, J., Zhu, Z., & Chen, D. (2023). Lowest Antarctic Sea Ice Record Broken for the Second Year in a Row. *Ocean-Land-Atmosphere Research*, 2, 0007. https://doi.org/doi:10.34133/olar.0007

Luo, H., Yang, Q., Mazloff, M., & Chen, D. (2023). A Balanced Atmospheric Ensemble Forcing for Sea Ice Modeling in Southern Ocean. *Geophys. Res. Lett.*, 50(5), e2022GL101139. https://doi.org/10.1029/2022GL101139

Luo, H., Yang, Q., Mu, L., Zhang, Z., Xi, J., Nerger, L., Mazloff, M., et al. (2021). DASSO: a data assimilation system for the Southern Ocean that utilizes both sea-ice concentration and thickness observations. *J. Glaciol.*, 67(266), 1235-1240. https://doi.org/10.1017/jog.2021.57

Marshall, J., Hill, C., Perelman, L., & Adcroft, A. (1997). Hydrostatic, quasi-hydrostatic, and nonhydrostatic ocean modeling. *J. Geophys. Res.: Oceans*, 102(C3), 5733-5752. https://doi.org/https://doi.org/10.1029/96JC02776

Massonnet, F., Goosse, H., Fichefet, T., & Counillon, F. (2014). Calibration of sea ice dynamic parameters in an ocean-sea ice model using an ensemble Kalman filter. *J. Geophys. Res.: Oceans*, 119(7), 4168-4184. https://doi.org/10.1002/2013JC009705

Massonnet, F., Mathiot, P., Fichefet, T., Goosse, H., Beatty, C. K., Vancoppenolle, M., & Lavergne, T. (2013). A model reconstruction of the Antarctic sea ice thickness and volume changes over 1980-2008 using data assimilation. *Ocean Model.*, 64, 67-75. https://doi.org/10.1016/j.ocemod.2013.01.003

Maykut, G. A. (1978). Energy exchange over young sea ice in the central Arctic. *J. Geophys. Res.*, 83(C7). https://doi.org/10.1029/JC083iC07p03646

Mazloff, M. R., Heimbach, P., & Wunsch, C. (2010). An eddy-permitting Southern Ocean state estimate. *J. Phys. Oceanogr.*, 40(5), 880-899. https://doi.org/10.1175/2009jpo4236.1

Mu, L., Nerger, L., Tang, Q., Loza, S. N., Sidorenko, D., Wang, Q., et al. (2020). Toward a data assimilation system for seamless sea ice prediction based on the AWI climate model. *J. Adv. Model. Earth Syst.*, 12(4), e2019MS001937. https://doi.org/10.1029/2019ms001937

Nerger, L., & Hiller, W. (2013). Software for ensemble-based data assimilation systems—Implementation strategies and scalability. *Comput. Geosci.*, 55, 110-118. https://doi.org/10.1016/j.cageo.2012.03.026

Nerger, L., Janjić, T., Schröter, J., & Hiller, W. (2012). A unification of ensemble square root Kalman filters. *Mon. Weather Rev.*, 140(7), 2335-2345. https://doi.org/10.1175/mwr-d-11-00102.1

Nie, Y., Uotila, P., Cheng, B., Massonnet, F., Kimura, N., Cipollone, A., & Lv, X. (2022). Southern Ocean sea ice concentration budgets of five ocean-sea ice reanalyses. *Clim. Dyn.* https://doi.org/10.1007/s00382-022-06260-x

Oke, P. R., & Sakov, P. (2008). Representation error of oceanic observations for data assimilation. *J. Atmos. Ocean. Technol.*, 25(6), 1004-1017. https://doi.org/10.1175/2007jtecho558.1

Pham, D. T. (2001). Stochastic methods for sequential data assimilation in strongly nonlinear systems. *Mon. Weather Rev.*, 129(5), 1194-1207. https://doi.org/10.1175/1520-0493(2001)129<1194:Smfsda>2.0.Co;2

Rodwell, M. J., Lang, S. T. K., Ingleby, N. B., Bormann, N., Holm, E., Rabier, F., et al. (2016). Reliability in ensemble data assimilation. *Q. J. R. Meteorol. Soc.*, 142(694), 443-454. https://doi.org/10.1002/qj.2663

Shi, Q., Yang, Q., Mu, L., Wang, J., Massonnet, F., & Mazloff, M. R. (2021). Evaluation of sea-ice thickness from four reanalyses in the Antarctic Weddell Sea. *The Cryosphere*, 15(1), 31-47. https://doi.org/10.5194/tc-15-31-2021

Shu, Q., Wang, Q., Song, Z., Qiao, F., Zhao, J., Chu, M., & Li, X. (2020). Assessment of Sea Ice Extent in CMIP6 With Comparison to Observations and CMIP5. *Geophys. Res. Lett.*, 47(9), e2020GL087965. https://doi.org/10.1029/2020gl087965

Tsujino, H., Urakawa, L. S., Griffies, S. M., Danabasoglu, G., Adcroft, A. J., Amaral, A. E., et al. (2020). Evaluation of global ocean–sea-ice model simulations based on the experimental protocols of the Ocean Model Intercomparison Project phase 2 (OMIP-2). *Geosci. Model Dev.*, 13(8), 3643-3708. https://doi.org/10.5194/gmd-13-3643-2020

Turner, J., & Comiso, J. (2017). Solve Antarctica's sea-ice puzzle. *Nature*, 547(7663), 275-277. https://doi.org/10.1038/547275a

Verdy, A., & Mazloff, M. R. (2017). A data assimilating model for estimating Southern Ocean biogeochemistry. *J. Geophys. Res.: Oceans*, 122(9), 6968-6988. https://doi.org/10.1002/2016jc012650

Wang, J., Luo, H., Yang, Q., Liu, J., Yu, L., Shi, Q., & Han, B. (2022). An Unprecedented Record Low Antarctic Sea-ice Extent during Austral Summer 2022. *Adv. Atmos. Sci.*, 39(10), 1591-1597. https://doi.org/10.1007/s00376-022-2087-1

Wang, J., Min, C., Ricker, R., Shi, Q., Han, B., Hendricks, S., et al. (2022). A comparison between Envisat and ICESat sea ice thickness in the Southern Ocean. *The Cryosphere*, 16(10), 4473-4490. https://doi.org/10.5194/tc-16-4473-2022

Wang, Y., Counillon, F., Bethke, I., Keenlyside, N., Bocquet, M., & Shen, M.-l. (2017). Optimising assimilation of hydrographic profiles into isopycnal ocean models with ensemble data assimilation. *Ocean Model.*, 114, 33-44. https://doi.org/10.1016/j.ocemod.2017.04.007

Worby, A. P., Geiger, C. A., Paget, M. J., Van Woert, M. L., Ackley, S. F., & DeLiberty, T. L. (2008). Thickness distribution of Antarctic sea ice. *J. Geophys. Res.: Oceans*, 113(C5). https://doi.org/10.1029/2007JC004254

Xu, Y., Li, H., Liu, B., Xie, H., & Ozsoy-Cicek, B. (2021). Deriving Antarctic Sea-Ice Thickness From Satellite Altimetry and Estimating Consistency for NASA's ICESat/ICESat-2 Missions. *Geophys. Res. Lett.*, 48(20), e2021GL093425. https://doi.org/10.1029/2021GL093425

Zhang, J., & Rothrock, D. A. (2003). Modeling global sea ice with a thickness and enthalpy distribution model in generalized curvilinear coordinates. *Mon. Weather Rev.*, 131(5), 845-861. https://doi.org/10.1175/1520-0493(2003)131<0845:Mgsiwa>2.0.Co;2

Zhang, L., Delworth, T. L., Yang, X., Zeng, F., Lu, F., Morioka, Y., & Bushuk, M. (2022). The relative role of the subsurface Southern Ocean in driving negative Antarctic Sea ice extent anomalies in 2016–2021. *Commun. Earth Environ.*, 3(1), 302. https://doi.org/10.1038/s43247-022-00624-1

Zhang, S., Harrison, M. J., Wittenberg, A., Rosati, A., Anderson, J. L., & Balaji, V. (2005). Initialization of an ENSO forecast system using a parallelized ensemble filter. *Mon. Weather Rev.*, 133(11), 3176-3201. https://doi.org/10.1175/mwr3024.1

List of Figures

Figure 1. Optimizations of DASSO. Panel (a) illustrates the variation of the localization radius with latitude. The diamond symbol and the thin lines on either side of it represent the zonal mean of the localization radius and twice the standard deviation of changes in the localization radius at the corresponding latitude. The fitting of these diamonds is depicted by the red curve, which represents a Gaussian function. Panel (b) showcases the variance of SIC observation error for DASSO. The Southern Ocean is divided into five sectors: the Weddell Sea (60°W~20°E), the Indian Ocean (20°E~90°E), the Pacific Ocean (90°E~160°E), the Ross Sea (160°E~130°W), and the Amundsen–Bellingshausen Sea (130°W~60°W).

Figure 2. The simulation of SIE climatology. Panel (a) illustrates the temporal evolution of SIE climatology in both observations and simulations. The blue, red, and yellow curves represent the observation, the ensemble mean of Assim, and the ensemble mean of Assim_opt, respectively. Additionally, the blue bar indicates twice the standard deviation of changes in the observed SIE over the corresponding period. Panel (b) presents the difference in SIE climatology between the simulation and the observation. Within each cell, the lower (upper) section on the main diagonal indicates the difference in SIE climatology between observation and Assim (Assim_opt). The presence of a cross denotes that the simulation error exceeds the uncertainties associated with the observations.

Figure 3. The simulation of SIE anomaly in the Southern Ocean and SIT in the Weddell Sea. Panel (a) illustrates the temporal evolution of SIE anomaly in both observations and simulations. The curves in blue, red, and yellow correspond to the observation, the ensemble mean of Assim, and the ensemble mean of Assim_opt, respectively. The shading emphasizes twice the ensemble spread of the corresponding simulation. Panel (b) provides the statistical analysis of SIT simulations compared to observations obtained from ULS in the Weddell Sea. The circle and diamond symbols represent Assim and Assim_opt, respectively. The size of the symbol indicates the observed SIT with a larger (smaller) symbol representing SIT greater (less) than 1m. Additionally, the color illustrates the correlation between the simulation and observation.

Figure 4. The SIV anomaly in the Southern Ocean and the potential contributors to changes in the SIV uncertainties in Assim_opt. Panel (a) demonstrates the temporal evolution of the ensemble mean of SIV anomaly, with the shading representing twice the ensemble spread. Panel (b) depicts the correlation between SIV anomaly and the area-weighted mean SSS anomaly in the Southern Ocean (i.e., south of 55°S) (represented by the blue), as well as the correlation between the change rate of SIV anomaly and the change rate of SIV anomaly induced by oceanic heat flux (represented by the red), within the Southern Ocean over various decades. The colored bars indicate the correlation passing the F-test at a 99% significant level.

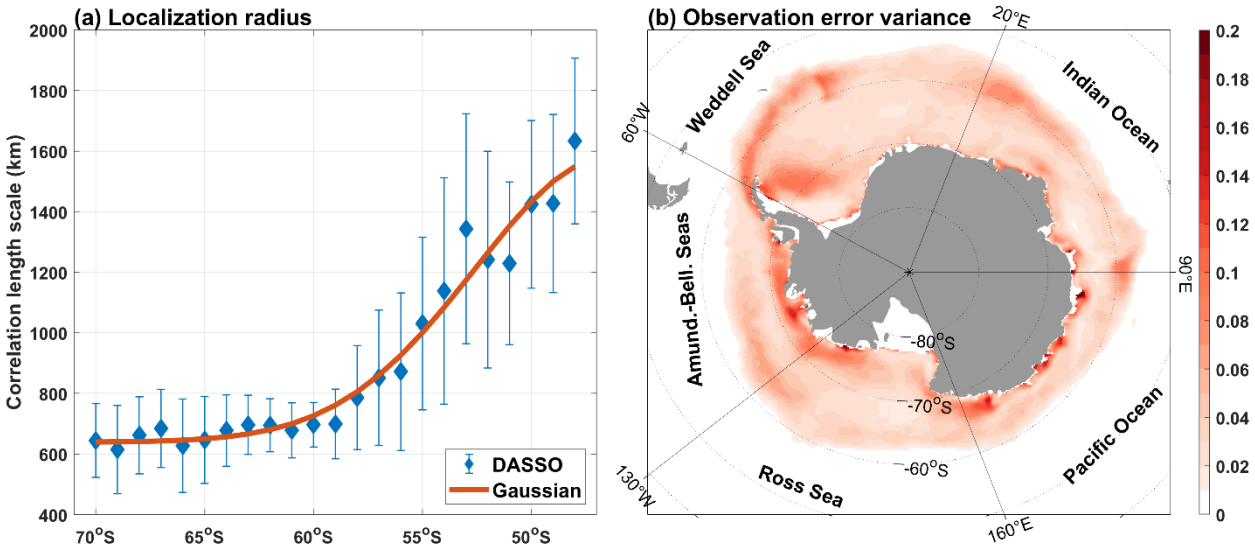

Figure 1. Optimizations of DASSO. Panel (a) illustrates the variation of the localization radius with latitude. The diamond symbol and the thin lines on either side of it represent the zonal mean of the localization radius and twice the standard deviation of changes in the localization radius at the corresponding latitude. The fitting of these diamonds is depicted by the red curve, which represents a Gaussian function. Panel (b) showcases the variance of SIC observation error for DASSO. The Southern Ocean is divided into five sectors: the Weddell Sea (60°W~20°E), the Indian Ocean (20°E~90°E), the Pacific Ocean (90°E~160°E), the Ross Sea (160°E~130°W), and the Amundsen–Bellingshausen Sea (130°W~60°W).

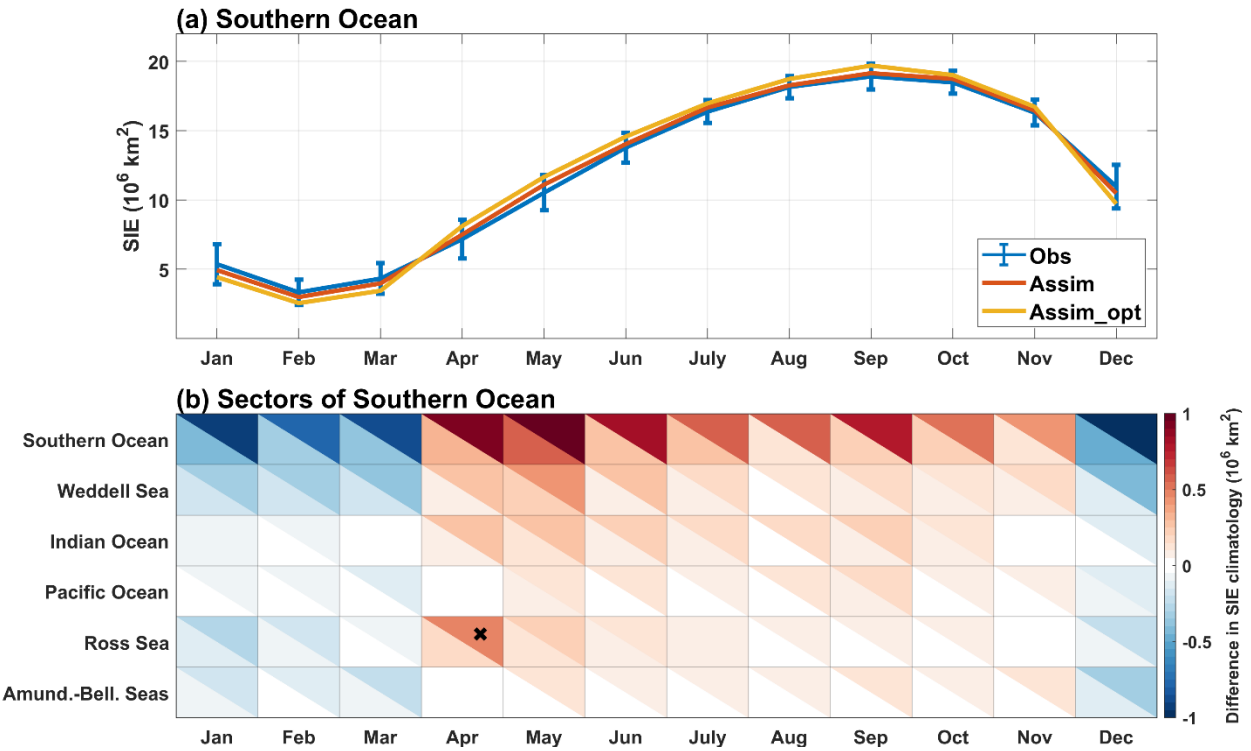

Figure 2. The simulation of SIE climatology. Panel (a) illustrates the temporal evolution of SIE climatology in both observations and simulations. The blue, red, and yellow curves represent the observation, the ensemble mean of Assim, and the ensemble mean of Assim_opt, respectively. Additionally, the blue bar indicates twice the standard deviation of changes in the observed SIE over the corresponding period. Panel (b) presents the difference in SIE climatology between the simulation and the observation. Within each cell, the lower (upper) section on the main diagonal indicates the difference in SIE climatology between observation and Assim (Assim_opt). The presence of a cross denotes that the simulation error exceeds the uncertainties associated with the observations.

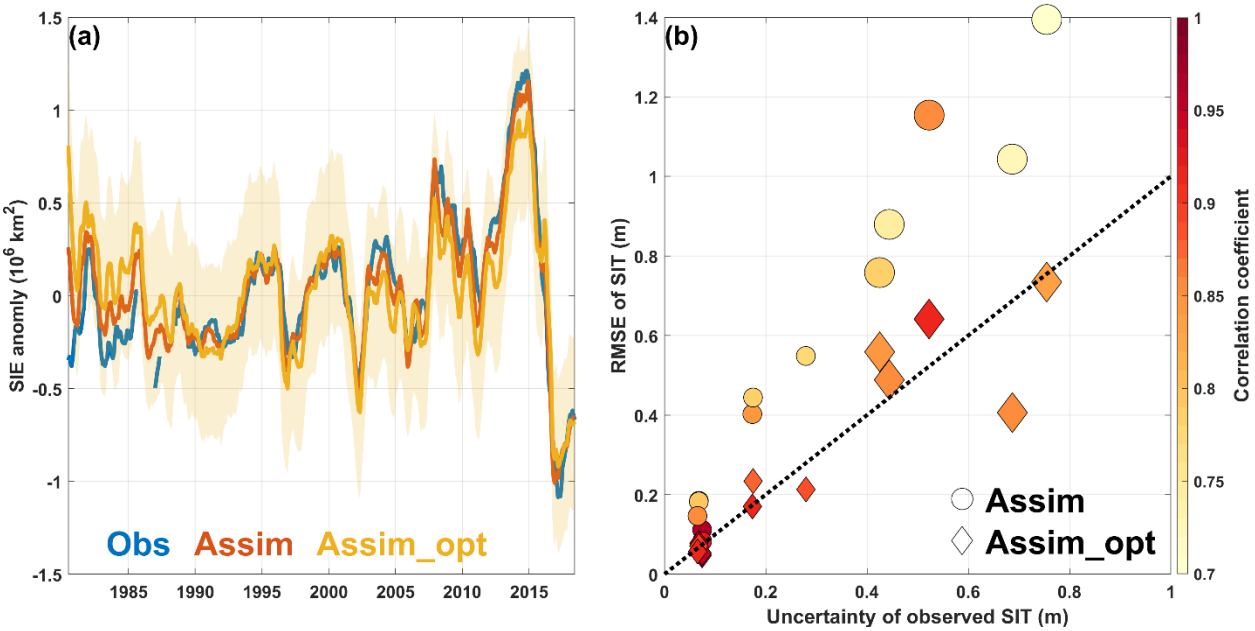

Figure 3. The simulation of SIE anomaly in the Southern Ocean and SIT in the Weddell Sea. Panel (a) illustrates the temporal evolution of SIE anomaly in both observations and simulations. The curves in blue, red, and yellow correspond to the observation, the ensemble mean of Assim, and the ensemble mean of Assim_opt, respectively. The shading emphasizes twice the ensemble spread of the corresponding simulation. Panel (b) provides the statistical analysis of SIT simulations compared to observations obtained from ULS in the Weddell Sea. The circle and diamond symbols represent Assim and Assim_opt, respectively. The size of the symbol indicates the observed SIT with a larger (smaller) symbol representing SIT greater (less) than 1m. Additionally, the color illustrates the correlation between the simulation and observation.

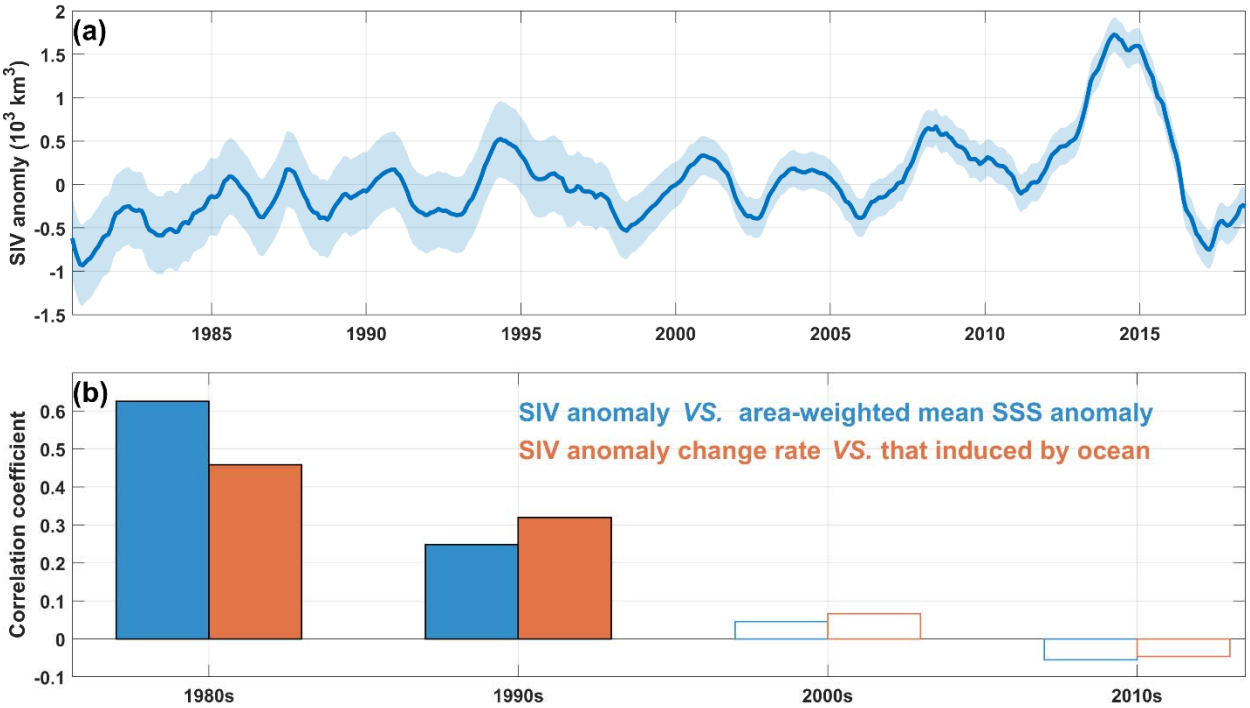

Figure 4. The SIV anomaly in the Southern Ocean and the potential contributors to changes in the SIV uncertainties in Assim_opt. Panel (a) demonstrates the temporal evolution of the ensemble mean of SIV anomaly, with the shading representing twice the ensemble spread. Panel (b) depicts the correlation between SIV anomaly and the area-weighted mean SSS anomaly in the Southern Ocean (i.e., south of 55°S) (represented by the blue), as well as the correlation between the change rate of SIV anomaly and the change rate of SIV anomaly induced by oceanic heat flux (represented by the red), within the Southern Ocean over various decades. The colored bars indicate the correlation passing the F-test at a 99% significant level.